CO-activator model for reconstructing Pt(100) surfaces: Local microstructures and chemical turbulence

Natalia Pavlenko
Institute for Condensed Matter Physics, Svientsitsky Street 1, 79011 Lviv, Ukraine
(Received 17 August 2007; revised manuscript received 14 December 2007; published 8 February 2008)

We present the results of the modeling of CO adsorption and catalytic CO oxidation on inhomogeneous Pt(100) surfaces which contain structurally different areas. These areas are formed during the CO-induced transition from a reconstructed phase with hexagonal geometry of the overlayer to a bulklike (1×1) phase with square atomic arrangement. In the present approach, the surface transition is explained in terms of nonequilibrium bistable behavior. The bistable region is characterized by a coexistence of the hexagonal and (1×1) phases and is terminated in a critical bifurcation point which is located at ($T_c\approx680$ K, $p^c_{\mathrm{CO}}\approx10$ Torr). Due to increasing fluctuations, the behavior at high temperatures and pressures in the vicinity of this cusp point should be qualitatively different from the hysteresis-type behavior which is typically observed in the experiments under ultrahigh vacuum conditions. On the inhomogeneous surface, we find a regime of nonuniform oscillations characterized by random standing waves of adsorbate concentrations. The resulting spatial deformations of wave fronts allow us to gain deeper insight into the nature of irregular oscillations on Pt(100) surface.

DOI: 10.1103/PhysRevE.77.026203 PACS number(s): 82.40.Bj, 82.45.Jn, 05.45.−a, 82.20.Wt

I. INTRODUCTION

The processes of surface reconstruction play a central role in heterogeneous catalysis [1]. A prominent example of a catalyst with the reactivity strongly affected by the rearrangement of the substrate atoms is the Pt(100) surface. The mechanism of such rearrangements is the tensile excess stress due to charge depletion of $5d$ orbitals of surface Pt atoms [2]. As a result, the bulklike (1×1) termination of clean Pt(100) corresponding to the square configuration of Pt atoms becomes metastable which causes a transformation to the hexagonal (hex) surface atomic arrangement. From the point of view of the catalytic properties, the crucial importance has the fact that such surface reconstructions are strongly affected by the adsorbates. The CO-induced lifting of the hex surface reconstruction and the stabilization of the (1×1) phase is forced by a gain in the CO adsorption energy and proceeds through the nucleation of (1×1) islands with high CO coverage [3–5].

The reconstruction of Pt surfaces is a key factor responsible for their complex oscillating behavior and pattern formation [6]. This is also supported by the fact that the stable Pt(111) surface where the reconstruction is not observed, does not exhibit oscillation properties. During the reconstruction, the surface of Pt(100) becomes inhomogeneous and contains coexisting micrometer-size regions of different (hex and square) atomic configurations. As demonstrated in low energy electron diffraction (LEED) studies [7–9], the propagating waves of surface modification can result in highly irregular spatiotemporal character of the oscillations.

Even with a constant oscillation period, the time variation of the local LEED intensity of small surface spots differs from the temporal behavior of the intensities integrated over the whole surface area [8]. Such a behavior is in contrast to the uniform oscillations on Pt(110) surfaces originating from the global coupling of various surface patches through the gas phase [6,8]. It should be noted that the mechanism of the global coupling has been extensively studied in a series of experimental works and by the theoretical modeling [10–16]. In distinction to Pt(110), the irregular oscillations during CO oxidation on Pt(100) possibly originate from the propagating chemical reaction fronts which can be triggered by defects and other surface imperfections [7,17]. The kinetic Monte Carlo simulations performed for the heterogeneous Pt(100) surfaces containing mesoscopic hex regions in macroscopic (1×1) surrounding, have essentially shown local unsynchronized oscillations [18]. These local oscillations disappear on the μm scale, whereas the experiment demonstrates well developed irregular oscillations even on the macroscopic mm scale [8]. Another aspect which can lead to the irregular temporal character of oscillations is the strong fluctuations on nm-size catalyst particles with (100) facets [19]. As the fluctuations in surface coverage are increasing with the decrease of the system size [20,21], they cannot satisfactorily explain the irregularities observed on single crystal surfaces of Pt(100).

To gain deeper insight into the nature of the irregular behavior, in the present work we consider a modeling of spatially inhomogeneous Pt(100) surfaces. In our approach, we account for the fact that the hex-square transformation occurs through a hysteresis and has a character of a first-order phase transition. Under the nonequilibrium conditions, the hysteresis features are described in terms of a bistable behavior which is characterized by a coexistence of the hex and square phases in a wide range of temperatures and partial pressures. Such a mechanism allows to obtain in a natural way the inhomogeneous surface state, without introducing additional separate variables for the description of the adsorbate coverage in different phases. Upon the increase of temperature and CO pressure, the bistable region narrows and terminates at a bifurcation cusp point ($T_c\approx680$ K, $p^c_{\mathrm{CO}}\approx10$ Torr). Due to strong fluctuations near this critical point, the behavior at high temperatures and pressures should be qualitatively different from the hysteresis-type behavior observed on Pt(100) under ultahigh vacuum conditions [4].

Furthermore, we address two main questions related to the surface inhomogeneities. First, we analyze the role of the

inhomogeneities in the nucleation and growth of adsorbate islands. We find that the difference between the CO desorption rates for the hex and square substrate geometries is responsible for the trapping of the adsorbed CO [3], a property responsible for the growth of CO islands during the hex-square transformation. Second, we study the oscillation behavior on inhomogeneous surface during the reaction of CO oxidation. We show that the surface inhomogeneities lead to the Benjamin-Feir instability and to a new inhomogeneous oscillating regime. This new regime is characterized by the random standing waves in spatially separated surface regions. We investigate the driving mechanisms of irregular oscillations and provide the analysis of the stability of the system with respect to nonuniform perturbations. The obtained deformations of the chemical wave fronts appear to be a direct consequence of structural inhomogeneities typical for Pt(100), and can be a possible clue for the explanation of the irregular oscillating behavior on this type of surfaces.

II. CO-ACTIVATOR MODEL AND ITS ANALYSIS

A fundamental property related to the adsorption of CO on low-index Pt(100) surfaces is a transformation of the initially stable reconstructed hex Pt surface into the bulklike (1×1) structure. The lifting of the surface reconstruction is activated in the case when the concentration (coverage) of adsorbed CO exceeds a critical value $\Theta^1_{\mathrm{CO}}\approx0.05$ monolayer (ML). In a wide range of the CO surface coverage $\Theta^1_{\mathrm{CO}}<\Theta_{\mathrm{CO}}<\Theta^2_{\mathrm{CO}}$ ($\Theta^2_{\mathrm{CO}}\approx0.3$ ML), the surface contains the coexisting areas of the (1×1) and hex geometry [5]. In the LEED experiments, the range of temperatures and CO partial pressures determining the phase coexistence is identified by a hysteresis behavior of LEED intensities [4].

It is noteworthy that in the nonequilibrium conditions, the hex-(1×1) coexistence should be described in terms of a bistable behavior. To provide a consistent analysis of the CO controlled bistability, we introduce a variable $A=\Theta_{\mathrm{CO}}$ for the description of the CO surface coverage and a parameter n which measures a degree of the surface reconstruction. The value $n=0$ corresponds to a fully reconstructed hex surface whereas the maximal value $n=1$ describes the recovered homogeneous (1×1) state.

Within the two-variables approach, the process of the CO-induced surface transformation contains two main stages. The first stage includes the change of the local mesoscopically averaged CO surface coverage during the steps of CO adsorption, desorption and CO diffusion on the Pt surface,

$$\frac{\partial A}{\partial t}=p_Ak_A[1-(A/A_s)^q]s_A-d_A\,A+D_A\Delta A. \tag{1}$$

Here p_A and k_A denote the partial pressure and the impingement rate of CO, respectively, and $A_s=0.5$ refers to the maximal (corresponding to a saturation) CO coverage; D_A is the CO diffusion coefficient. The factor $q>1$ models the precursor-type kinetics of the CO adsorption [22,23]. In our analysis, a typical value $q=3$ for the precursor factor is chosen.

For the kinetic processes on the inhomogeneous surface containing a mixture of hex and (1×1) islands, we need to consider two different contributions to the adsorption-desorption steps in (1). These two different types originate from the processes $\mathrm{CO}_{\mathrm{gas}}\leftrightarrow\mathrm{CO}_{\mathrm{hex}}$ and $\mathrm{CO}_{\mathrm{gas}}\leftrightarrow\mathrm{CO}_{1\times1}$ which contribute with the weights $(1-n)$ and n to the total rates of surface adsorption and desorption. As a consequence, the final expression for the CO sticking and CO desorption coefficients s_A and d_A contain both contributions

$$s_A=s_A^0(1-n)+s_A^1n,$$

$$d_A=d_A^0(1-n)+d_A^1n, \tag{2}$$

where $d_A^0=\nu_0\exp(-E_d^0/RT)$ and $d_A^1=\nu_1\exp(-E_d^1/RT)$. In the expressions for s_A and d_A, the parameters s_A^0, d_A^0 and s_A^1, d_A^1 are the CO sticking and desorption coefficients in the hex and (1×1) phases, respectively. As is shown in [5], the low desorption rate d_A^1 is a prime factor responsible for high CO coverage's of the (1×1) surface. In contrast, due to higher desorption rate on the hex surface, a significant part of adsorbed CO molecules desorps which leads to substantially lower CO coverage's in the hex state.

For the sticking coefficients, we use the values $s_A^0=0.75$ ($A=0.05$, hex geometry) and $s_A^1=0.34-0.7$ ($A=0.5-0.3$, 1×1 geometry) reported in Ref. [4]. In the Arrhenius-type form of the desorption coefficients d_A^0 and d_A^1 we choose the following values for the rate parameters: $\nu_0=4\times10^{13}$ s^{-1} and $\nu_1=3\times10^{15}$ s^{-1}; $E_d^0=27.5$ kcal/mol and $E_d^0=34.5$ kcal/mol [4].

Furthermore, in our approach we consider the transformation of the substrate state activated by the adsorbed CO. In the two-variable model, the time evolution of the local mesoscopically averaged surface state parameter n is described by the following phenomenological equation:

$$\frac{\partial n}{\partial t}=\gamma_{01}\,n(1-n)(A/A_s)\,\Theta(A-A_c^1)-\gamma_{10}\,n(1-A/A_s)^2+\kappa\Delta n. \tag{3}$$

Here the first term refers to the lifting of the hex reconstruction. The rate of the lifting is proportional to the CO coverage a and to the factor $\gamma_{01}n(1-n)$ which is a mean-field form of the effective flux between the hex and (1×1) regions. By introducing the step function $\Theta(A-A_c^1)$ [$\Theta(\xi)=1$ for $\xi>0$ and 0 otherwise], we account for the experimental observation that the transition to the (1×1) phase does not occur below a critical coverage $A_c^1=\Theta_{\mathrm{CO}}^1$. In our calculations, we describe the transition rate $\gamma_{01}=\nu_{01}\exp(-E_{01}/RT)$ by an Arrhenius-type expression where the activation energy $E_{01}\sim2$ kcal/mol corresponds to a small activation barrier for the transformation from the hex to the (1×1) state [4], and the prefactor $\nu_{01}\approx10$ s^{-1} gives correct time scales for the transformation in the considered temperature interval [22,24].

The second term in (3) refers to the reverse $(1\times1)\rightarrow$hex reconstruction with a rate coefficient γ_{10}. Here the factor $(1-A/A_s)^2$ accounts for the property that the reconstruction can occur locally if a small cluster of neighboring

surface positions (a pair in the simplest case) is not occupied by adsorbed CO which is in analogy with the assumption considered in [18,25].

For an inhomogeneous surface, the Laplacian term Δn in (3) originates from the contribution of the interfaces between different surface geometries to the total system energy [26,27]. Consequently, the coefficient κ describes the energy costs of such interfaces and is related to the characteristic interface width $L_n=\sqrt{\kappa/\gamma_{01}}$ which is typically of the order of a few nanometers. We note that the characteristic diffusion length of the adsorbed CO is given by $L_A=\sqrt{D_A/\gamma_{01}}$ and is of the order of several micrometers. The fast CO diffusion between the hex and (1×1) areas described by the diffusion term in (1), controls the μm size of CO islands which is discussed in details in Sec. III.

Equations (1) and (3) can be transformed by the substitution

$$A = a\,A_s, \quad x = \tilde{x}L_A, \quad \tilde{d}_A = d_A/\gamma_{01}, \quad \tilde{t} = t\gamma_{01},$$

$$\tilde{p}_A = p_A k_A/A_s\gamma_{01}, \quad \eta = \kappa/D_A, \quad \gamma = \gamma_{10}/\gamma_{01}, \tag{4}$$

into the following dimensionless form:

$$\frac{\partial a}{\partial \tilde{t}} = f_1(a,n) + \Delta_{\tilde{x}} a,$$

$$\frac{\partial n}{\partial \tilde{t}} = f_2(a,n) + \eta\Delta_{\tilde{x}} n, \tag{5}$$

where

$$f_1 = \tilde{p}_A(1-a)s_A - \tilde{d}_A\, a,$$

$$f_2 = n(1-n)a\,\Theta(a-a_c^1) - \gamma n(1-a)^2. \tag{6}$$

For a given $a\neq 0$, the second equation (5) leads to the two stable steady states, $n_1=0$ and $n_2=1-\gamma(1-a)^2/a$. In the limit $a\to 1$, the second solution approaches the value $n_2=1$ which implies the full lifting of the hex geometry by the CO adsorption. In the following discussion, we will omit for convenience the tilde signs in the notations of dimensionless time and coordinate.

A remarkable property of the system (2), (5), and (6) is a strong dependence of the CO adsorption and desorption rates on the local configurational state of the surface determined by the parameter n. In analogy to [5], this dependence can be conveniently analyzed in terms of a net sticking probability of CO molecules defined as

$$s_A^n = s_A - \tilde{d}_A a/\tilde{p}_A(1-a). \tag{7}$$

Specifically, despite a large initial sticking coefficient s_A^0 in the hex regions, the significant contribution of the second desorption term in (7) results in a suppression of s_A^n which reflects the fact of low CO coverage $A\leq 0.05$ ML observed on the reconstructed surfaces. In contrast, due to the low desorption rates on the (1×1) substrate, the adsorption of CO will result in large values of s_A^n and consequently in high CO coverage in the regions with the lifted reconstruction. In the following analysis, we will use the net sticking probability as a relevant quantity for the interpretation of the growth kinetics of CO islands on inhomogeneous substrates.

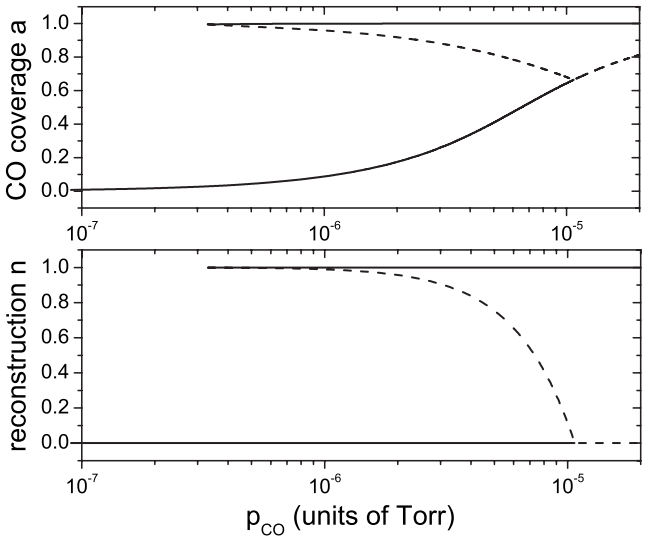

FIG. 1. Stationary CO coverage a and surface reconstruction parameter n versus CO pressure. Here $T=450$ K. The unstable solutions correspond to the saddle nodes and are indicated by dashed curves.

Surface transition between hex and (1×1) on Pt(100): Bistable behavior. A central feature of the models (5) and (6) is the occurrence of a bistable region characterized by the coexistence of the states n_1 and n_2 with low and high CO coverage. In the analysis of (5) and (6), we choose $k_A=1.13\times10^5$ s^{-1} Torr^{-1} ML and perform the calculations of the steady states using the rate parameter $\gamma_{10}=\nu_{10}\times\exp(-E_{10}/RT)$ with $E_{10}=23$ kcal/mol and $\nu_{10}=10^{12}$ s^{-1}. The large value of E_{10} is consistent with the high activation barrier for the hex reconstruction of the clean Pt(100) surface reported in [4]. In the Arrhenius form of the desorption rate parameter d_A^1 of the (1×1) substrate, we choose the values $\nu_1=1\times10^{15}$ s^{-1} and $E_d^1=37$ kcal/mol. These values have been deduced in [4] from the temperature dependences of the corresponding LEED intensities which exhibit a hysteresis-type behavior.

Figure 1 shows the stationary solutions calculated for different CO pressures. Here the bistable region where the stable hex and (1×1) phases coexist is located in the range of pressures between $p_A^1=3\times10^{-7}$ Torr and $p_A^2=10^{-5}$ Torr.

The regions of the stability of different phases together with the bistable region are indicated on the phase diagram $(1/T, p_{CO})$ shown in Fig. 2. We note that the topology of the diagram and the location of the bistable region agree well with a LEED diagram obtained by the estimation of isosteric heats of CO adsorption [4]. A remarkable feature of our diagram is that the bistable region narrows with the increasing p_{CO} and terminates at a critical bifurcation point at $p_{CO}^c\approx2\times10^1$ Torr and $T_c\approx680$ K. The existence of such a cusp point on the diagram is a clear manifestation of the critical behavior which is associated with a strong increase of near-critical fluctuations in the system. We should emphasize that in this high pressure range, the direct comparison with the

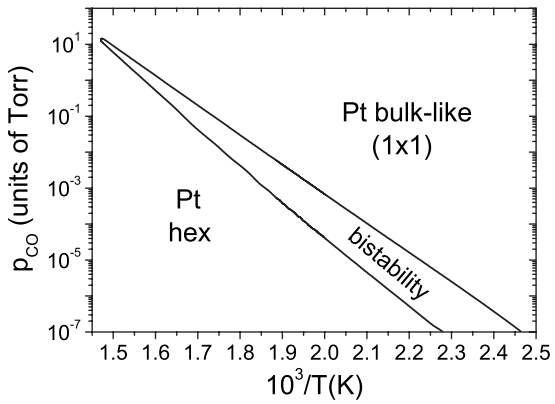

FIG. 2. Phase diagram $(1/T, p_{CO})$ showing the regions of the stability of the hex and (1×1) phases with the indication of the bistable region where both these phases coexist on Pt surface.

experimental data obtained at low CO pressures up to 10^{-4} Torr cannot be provided. In view of this, additional experimental studies conducted at high pressures and temperatures are required in order to verify the existence of the obtained critical bifurcation point. For Pt(100), such experiments would be of a central importance in bridging a "pressure gap" between the hysteresis-type behavior at low p_{CO} and possible critical fluctuations which should exist at high CO pressures.

III. ISLANDS NUCLEATION ON INHOMOGENEOUS PT SURFACE

In the bistable region, the problem of prime interest is the behavior of adsorbate molecules on a surface which contains micrometer-size areas of different geometry. To study the nucleation and growth of adsorbate islands on such an inhomogeneous substrate, we must consider the full set of the reaction-diffusion equations (5) and (6). It should be noted that the strong difference between the characteristic nanoscale width of the hex/(1×1) interfaces L_n and the micrometer scale of the CO diffusion length L_A results in small values of the ratio η in (4) which is of the order 10^{-3}–10^{-4}. Furthermore, in our analysis we choose a typical value $\eta=0.005$. Equations (5) and (6) have been solved numerically using an implicit two-level finite-difference scheme on a discrete finite grid with the Neumann boundary conditions $\partial a/\partial x=0$, $\partial n/\partial x=0$. In this absolutely stable scheme, the standard finite difference approximations of the second-order accuracy for coordinate derivatives and the first-order accuracy approximation for time derivatives are applied.

To demonstrate the influence of the surface geometry on the growth of adsorbate islands, in Fig. 3 we present the spatiotemporal evolution of islands with high CO coverage on the inhomogeneous surface. For simplicity, we consider a quasi-one-dimensional case described by the spatial coordinate x which corresponds to a stripelike surface patterning. The initial geometry of the substrate is characterized by two symmetric regions exhibiting a high degree of transformation into the (1×1) phase with $n=0.5$. These regions of the

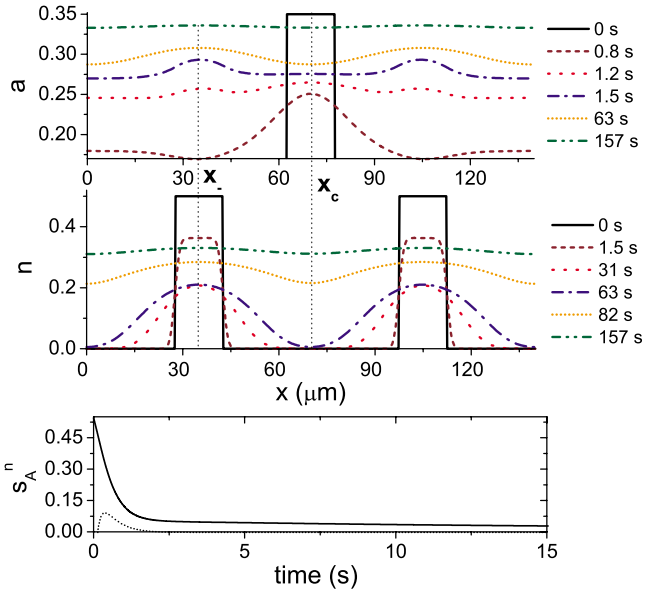

FIG. 3. (Color online) Time evolution of spatial profiles of a and n on inhomogeneous Pt surface for $p_A=3.3\times10^{-6}$ Torr, $\eta=0.005$, $\gamma=0.5$, and $T=450$ K. The nucleation and growth of two islands with high a coverage occurs in the 1×1 surface regions. The bottom panel shows the behavior of the net CO sticking probabilities in the central hex $(x=x_c)$ and in the unreconstructed $(x=x_-)$ parts of the substrate.

length 15 μm are located at a distance about 35 μm from the center and surrounded by the reconstructed (hex) areas with $n=0$. In the central region, we initially have a preformed CO island which is centered at $x=x_c$ and located in the hex area beyond the (1×1) patches. Furthermore, in the process of the temporal evolution shown in Fig. 3, the CO coverage of the central hex area decreases. This decrease is driven by the CO desorption which is dominant due to the high desorption coefficient d_A^0. It is remarkable that the disappearance of the central CO island is accompanied by the simultaneous development of two new symmetric islands with high CO coverage. These two islands nucleate in the (1×1) parts of the substrate where the desorption is suppressed and CO molecules become trapped due to the high CO binding energy on the surface.

The corresponding difference between the kinetic properties of different regions of inhomogeneous substrate can be interpreted in terms of the time evolution of the net sticking probabilities s_A^n shown in the bottom panel of Fig. 3. The predominant desorption of CO from the central hex area is reflected in the initial zero net sticking probability $s_A^n(x=x_c)$ which slightly increases with the expansion of the (1×1) areas on the surface. In contrast to this, in the symmetric regions with partially lifted surface reconstruction, the net sticking probability is high due to low desorption rates on these parts of the surface $[s_A^n(x=x_-)$ in Fig. 3].

In fact, the obtained simultaneous disappearance and nucleation of CO islands in the areas of different geometry can be characterized as an effective island propagation. The basic mechanism responsible for this propagation, is the difference between the CO desorption rates in the (1×1) and

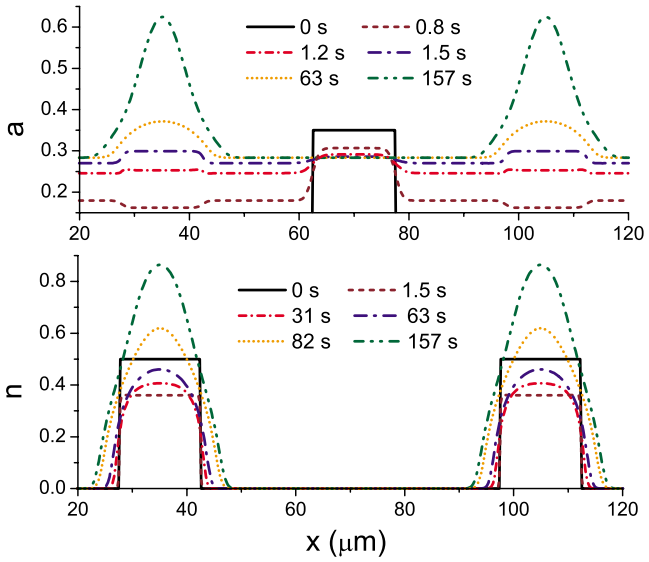

FIG. 4. (Color online) Time evolution of spatial profiles of a and n on inhomogeneous Pt surface for $p_A=3.3\times10^{-6}$ Torr, $\gamma=0.5$, and $T=450$ K. The CO diffusion constant D_A is by two orders of magnitude smaller than that in Fig. 3. To provide a correct comparison of both spatial profiles, the parameter scaling is performed relative to the reference data in Fig. 3.

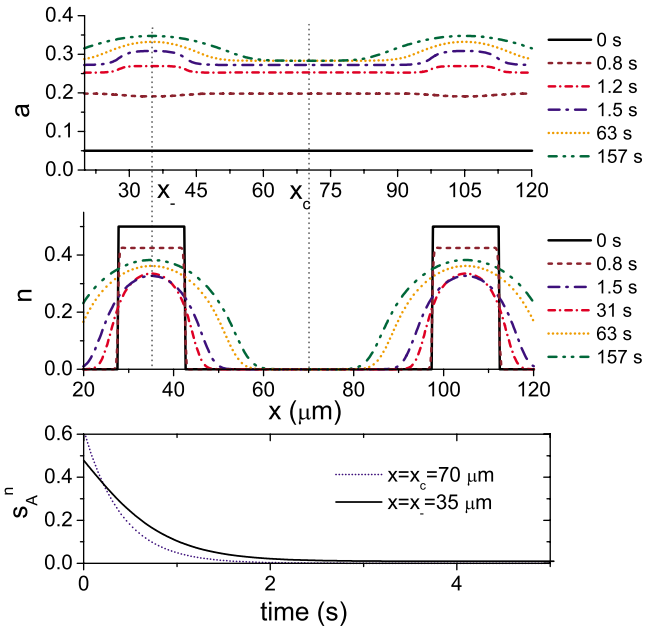

FIG. 5. (Color online) Time evolution of spatial profiles of a and n on inhomogeneous Pt surface for $p_A=3.3\times10^{-6}$ Torr, $\gamma=0.5$, and $T=450$ K. The CO diffusion constant D_A is by one order of magnitude smaller then that in Fig. 3. The initial spatial distribution of CO is homogeneous with $a=0.05$. To provide a correct comparison of both spatial profiles, the parameter scaling is performed relative to the reference data in Fig. 3. The bottom panel shows the behavior of the net CO sticking probabilities in the central hex ($x=x_c$) and in the unreconstructed ($x=x_-$) parts of the substrate.

hex surface parts. Consequently, in the (1×1) regions where the desorption rate is lower, the rapid CO diffusion between the hex and (1×1) areas results in the trapping of CO molecules and in the growth of the micrometer-size islands.

The effect of the CO diffusion on the island growth becomes more clear when we perform calculations with a small CO diffusion coefficient which corresponds to the case shown in Fig. 4. In Fig. 4, the decrease of D_A by the two orders of magnitude corresponds to the additional prefactor 10^{-2} near the diffusion term in (5). The comparison with Fig. 3 clearly shows that such a slow diffusion leads to a strong localization of the new symmetric CO islands in the (1×1) areas and to a significant slowing down of the hex-lifting process.

To analyze the role of the CO desorption in the island nucleation, we consider an inhomogeneous surface where the initial CO coverage is uniformly distributed with $a(x)=a_0=0.05$ (Fig. 5). This is lower than the critical coverage $a_c^1=0.1$ necessary for the hex$\rightarrow(1\times1)$ transition. In the course of temporal evolution, the CO coverage begins to increase predominantly in the (1×1) regions of substrate which leads to the development of two symmetric CO islands. Although the absolute sticking coefficient in the (1×1) areas s_A^1 is smaller that the hex sticking coefficient s_A^0, the low CO desorption rates lead to substantially higher net CO sticking probability in the (1×1) regions, which is illustrated by the time evolution of s_A^n in the hex $(x=x_c)$ and (1×1) $(x=x_-)$ regions in Fig. 5 (bottom panel). It should be noted that the obtained strong dependence of the net sticking probabilities on the geometry of the substrate is in agreement with the scenario of CO island growth dynamics discussed in [5]. In view of this, the difference in the CO desorption rates appears to be a central mechanism responsible for the CO island nucleation and CO trapping on inhomogeneous surfaces.

IV. MODELING CATALYTIC CO OXIDATION

Equations (1) and (3) represent in fact a CO-activator model where the surface transition hex$\rightarrow(1\times1)$ is activated by the CO adsorption. On the Pt(100) surfaces, this structural surface transformation is a key source for complex spatial self-organization and temporal oscillations observed in surface reactions, such as catalytic CO oxidation [7,8]. This is in distinction to the oscillating behavior on Pt(110) surfaces where the oscillations occur via a coupling through the gas phase. For Pt(100), the basic oscillation mechanism consists in a periodic switch between the phases with low and high reactivity. This switch is related to the periodic surface transformation between the hex and (1×1) surface structures. We note that in contrast to the adsorbed CO which activates the hex$\rightarrow(1\times1)$ transformation in the considered temperature interval 400–500 K, the coadsorbed oxygen plays a role of inhibitor. The inhibiting function in this case is based on the fact that the oxygen predominantly adsorbs in the unreconstructed (1×1) phase and reacts with the adsorbed CO. The consequent decrease of the CO coverage during the reaction drives the reverse $(1\times1)\rightarrow$hex surface reconstruction. In this context, the inhibiting character of the oxygen is a basis for the oscillatory behavior in the modeling of the surface CO oxidation.

Oscillating behavior. To study the role of the adsorbed oxygen, we introduce the additional equation for the description of the oxygen coverage $B=\Theta_O$ on the Pt surface,

$$\frac{\partial B}{\partial t} = p_B k_B s_B\, n\left(1-\frac{A}{A_s}-\frac{B}{B_s}\right)^2 - r\,AB, \tag{8}$$

where $p_B=p_{O_2}$ and k_B refer to the O_2 partial pressure and impingement rate, respectively. As the O_2 sticking coefficient in the hex phase is negligibly small, the surface state parameter n in the first term restricts the oxygen adsorption to the unreconstructed (1×1) parts of the substrate, which occurs with the sticking coefficient $s_B=0.3$. The mean-field factor $(1-A/A_s-B/B_s)^2$ accounts for the condition that two neighboring surface positions not occupied by CO_{ads} and O_{ads} are required for the dissociative adsorption of O_2. The second term in (8) describes the decrease of B due to the reaction with CO_{ads}, with the reaction rate $r=r_0\exp(-E_r/RT)$. The similar reaction term is also included into the kinetic equation (1) for the CO coverage. In our analysis of CO oxidation, we choose the values $r_0=2\times10^{10}$ s^{-1} ML^{-1} and $E_r=24.1$ kcal/mol for the reaction parameters. As the diffusion coefficient of the adsorbed oxygen is about from three to four orders of magnitude lower than the CO diffusion parameter D_A, the adsorbed oxygen is considered as immobile [28].

After introducing the dimensionless forms for the oxygen coverage $b=B/B_s$, oxygen partial pressure $\tilde{p}_B=p_Bk_Bs_B/\gamma_{01}B_s$, and for the reaction rate $\tilde{r}=r/\gamma_{01}$, Eq. (8) can be rewritten in the form

$$\frac{\partial b}{\partial \tilde{t}} = f_3(a,n,b) = \tilde{p}_B\, n(1-a-b)^2 - \tilde{r}A_s a\, b. \tag{9}$$

In Eq. (5), the modified function $f_1(a,n,b)$ now includes the reaction term $f_1=\tilde{p}_A(1-a)s_A-d_Aa-\tilde{r}B_sa\,b$.

To analyze the stability of the macroscopically homogeneous solutions of (5) and (9), we performed a linearization of the system in the vicinity of the stationary states $\boldsymbol{\xi}_0=(a_0,n_0,b_0)^T$. In this approach, the small deviations $\delta\boldsymbol{\xi}=(\delta a,\delta n,\delta b)^T$ from $\boldsymbol{\xi}_0$ can be determined from the system of equations

$$\delta\dot{\boldsymbol{\xi}} = G\,\delta\boldsymbol{\xi}, \tag{10}$$

where $G=\{g_{i,l}\}$ is the matrix of the derivatives $g_{i,l}=\partial f_i/\partial\xi_l|_{\boldsymbol{\xi}_0}$.

Furthermore, the stability analysis can be reduced to the calculation of the Lyapunov exponents λ_j (eigenvalues of G) with the corresponding deviation vectors (eigenvectors) $\delta\boldsymbol{\xi}_j$, so that $G\,\delta\boldsymbol{\xi}_j=\lambda_j\boldsymbol{\xi}_j$ $(j=1,2,3)$. From Eq. (10), we can easily obtain the expressions for the time evolution of the eigenvectors $\delta\boldsymbol{\xi}_j$, $\delta\boldsymbol{\xi}_j=\boldsymbol{c}_j^0\exp(\lambda_jt)$, where the constants $\boldsymbol{c}_j^0$ should be found from the initial conditions. As a consequence, each arbitrary deviation $\delta\boldsymbol{\xi}(t)$ can be represented as $\delta\boldsymbol{\xi}=\Sigma_jc_j\delta\boldsymbol{\xi}_j$ and in this way is fully determined by λ_j.

In the analysis of the monostable, bistable, and oscillation states, the Lyapunov exponents have been calculated numerically. Figure 6 shows an example of the oscillating behavior in the vicinity of a subcritical Hopf bifurcation point. Here, for larger p_A, the real part of two complex conjugated

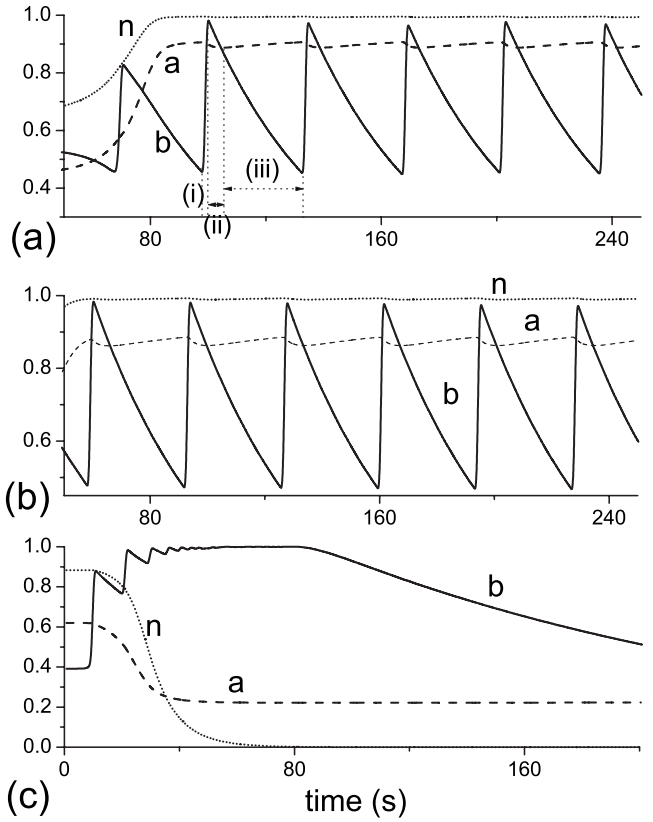

FIG. 6. Time evolution of dimensionless CO and oxygen coverage a and b and of the surface state parameter n at various CO pressures $p_{CO}=p_A$. The cases (a), (b), and (c) correspond to the values of the CO pressure $p_A=3.2\times10^{-6}$ Torr, $p_A=2.8\times10^{-6}$ Torr, and $p_A=2.58\times10^{-6}$ Torr, respectively. Here $p_{O_2}=p_B=5\times10^{-5}$ Torr, $k_B=5.6\times10^5$ ML $Torr^{-1}$ s^{-1}, $\gamma=0.5$, and $T=450$ K. The stages (i)–(iii) on the top panel form a single oscillation cycle.

Lyapunov exponents $\mathrm{Re}\,\lambda_2=\mathrm{Re}\,\lambda_3>0$ corresponds to an unstable limit cycle in the phase space determined by the vectors $\boldsymbol{\xi}=(a,n,b)^T$. Such a cycle involves several kinetic stages which are based on a complex interplay between the CO-activator-induced hex$\rightarrow(1\times1)$ transformation, and the inhibitor-caused reverse decrease of the adsorbate coverage resulting in the hex surface reconstruction.

Figure 6 demonstrates how the periodic oscillations of the coverage's a and b are related to the surface transformation described by the parameter n. The increase of the oxygen coverage b up to a saturation value $b=1$ results in a suppression of the oxygen adsorption [stage (i) in the top panel in Fig. 6]. Consequently, the reaction step becomes dominating and leads to a decrease of the oxygen coverage b. During the CO oxidation, the decreasing CO coverage a results in the reverse hex reconstruction of the surface, a process reflected by a slight decrease of the state parameter n [stage (ii) in Fig. 6]. The reconstruction continues until the CO adsorption begins to prevail and the CO-activated hex$\rightarrow(1\times1)$ transformation starts again [stage (iii) in Fig. 6]. At this stage, the increase of the oxygen adsorption in the (1×1) phase results in a repeat of the oscillation cycle.

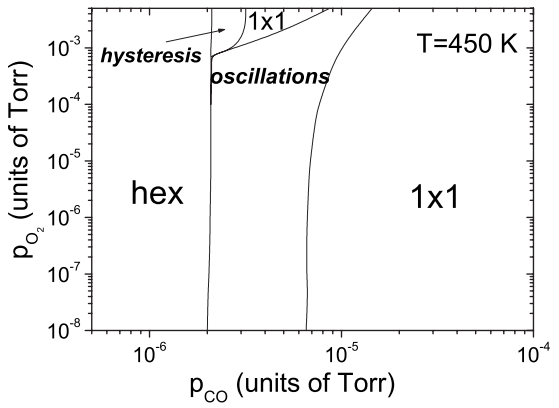

FIG. 7. Bifurcation phase diagram (p_{CO}, p_{O_2}) calculated at $T=450$.

As is demonstrated in the bottom panel of Fig. 6, the decrease of the CO pressure p_A leads to the disappearance of the oscillations and to a further convergence of the system state to a monostable hex phase.

Figure 7 presents a bifurcation phase diagram (p_A, p_B) calculated at $T=450$ K with the indicated areas of monostable, bistable, and oscillating behavior. One can see that the oscillating region extends with the increasing p_B which supports a key role of the oxygen in the development of the oscillations. Another remarkable feature is that the region where the oscillations occur coincides with the region of the structural surface transformation which is in full agreement with the experimental observations by LEED [8].

In the diagram shown in Fig. 7, the oscillating regime disappears in the limit $p_B \to 0$ which corresponds to the absence of the adsorbed oxygen on the surface. It should be noted that even at extremely low oxygen partial pressures $p_B < 10^{-7}$ Torr, the calculations still give a region with low oscillation amplitudes induced by small nonzero b. This is in contradiction to the experimental indications of the disappearance of oscillations for $p_B < p_A$, a property explained in terms of a blocking of the adsorption sites by CO [8]. Due to a mean-field form of the equations used in our modeling, even at low pressures $p_B < 10^{-7}$ Torr we find a small nonzero b which leads to the existence of the oscillations. To improve the results in this range of pressures, more precise methods must be applied. A possible way to account for the blocking of the adsorption sites by CO would be to perform Monte Carlo simulations which will require further numerical investigations.

The crucial difference between the oscillations on Pt(100) and Pt(110) is related to their spatiotemporal behavior. While Pt(110) oscillations arise due to the coupling through the gas phase and have a well developed regular character, the oscillations on Pt(100) are in general irregular. This irregularity is usually explained by the inhomogeneous nature of Pt(100) surfaces, where the waves of structural transformation develop on structurally different surface patches at different time intervals [8]. Due to a weak spatial coupling via the surface diffusion, the resulting integrated oscillation profiles are nonuniform and highly irregular [9].

To gain more insight into the nature of irregularities on Pt(100), one needs to study comprehensively the oscillations on surfaces which contain patches of different geometries and characterized by different levels of adsorbate coverage. In fact, such studies can be considered in a more wide context, since the modern lithographic techniques give a possibility to prepare prepatterned surfaces [6]. Moreover, the control of adsorbate coverage can be achieved by the methods of scanning tunneling microscopy and laser-induced thermal desorption which create artificial micrometer-size microstructures on the surfaces [29]. In this way, the character of the oscillating behavior can be probed and externally tuned.

V. CONSEQUENCE OF SURFACE INHOMOGENEITIES: CHEMICAL TURBULENCE

To study the effect of inhomogeneities, we consider a one-dimensional substrate of a size L_x. The substrate contains a partially reconstructed central surface region $\mathcal{C}$ surrounded by the (1×1)-surface parts where the hex phase is fully lifted. For $x\in\mathcal{C}$, the initial surface state is described as $n(x,t=0)=n_p<1$. On the substrate, the region $\mathcal{C}$ has the length $2\Delta\leq L_x$ and is defined as $|x-x_c|\leq\Delta$ where x_c is the center of the substrate. In our analysis, we choose the following initial conditions for the surface coverage:

$$b(x,t=0)=\begin{cases} b_p, & x\in\mathcal{C}, \\ 0, & |x-x_c|>\Delta, \end{cases} \qquad a(x,t=0)=a_p. \tag{11}$$

Inside $\mathcal{C}$, the temperature, reaction-diffusion parameters and the initial conditions $\boldsymbol{\xi}_p=(a_p,n_p,b_p)^T$ correspond to the homogeneous oscillating state close to the subcritical Hopf bifurcation point. This implies that in the case when $\mathcal{C}$ will cover the entire substrate $(2\Delta=L_x)$, the time behavior is characterized by the homogeneous periodic oscillations of the state parameter $n(x,t)=n(t)$ and of the surface coverage's $a(x,t)=a(t)$ and $b(x,t)=b(t)$ already considered in the preceding section. In contrast, in the case when the oscillating surface region $\mathcal{C}$ is located inside the unreconstructed surface area, the gradients of the adsorbate coverage's and of the state parameter n near the hex/(1×1) interfaces at $x=x_\pm$ lead to the transition to a highly nonuniform state. To see this, in Figs. 8 and 9 we present the evolution of the substrate geometry and adsorbate coverage for a case when $2\Delta=40$ μm$<L_x=70$ μm. One can clearly observe the development of a completely new inhomogeneous surface state. In this state, the initial spatial plateaulike distribution of b is broken. Moreover, the profiles of the oxygen coverage b can be identified as inhomogeneous oscillating standing waves. At the first stages of the time evolution ($t<38$ s in Fig. 8), these standing patterns are localized predominantly within $\mathcal{C}$. Furthermore, the additional irregular patterns develop near the substrate boundaries due to strongly increased b, which leads to a final extension of the inhomogeneous oscillations well beyond $\mathcal{C}$ on the entire substrate (cases $t=110$ and 472 s in Fig. 8). The breaking of the homogeneous oscillating regime corresponds to the Benjamin-Feir instability of homogeneous $(k\to0)$ oscillating waves. The appearing irregular spatial patterns are characterized by a deformation of the

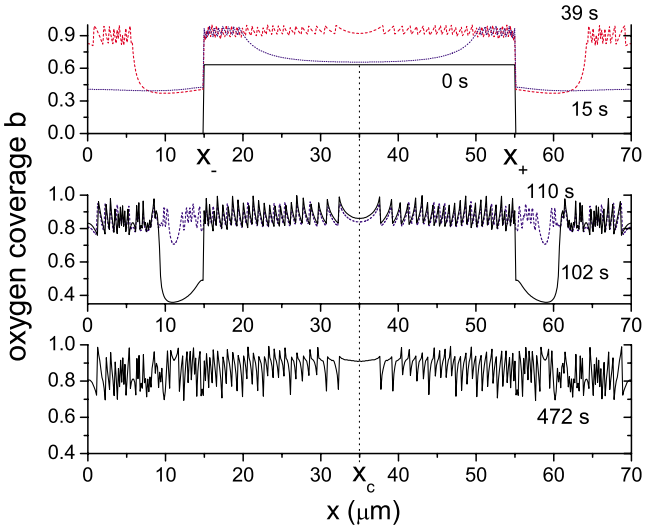

FIG. 8. (Color online) Time evolution of spatial profiles of the oxygen coverage b. The initial distribution of b is steplike with $b=b_p=0.63$ inside the central region $\mathcal{C}$ of a length $2\Delta=40$ μm with $x_c=35$ μm and $b=0$ beyond this region. Here $p_A=6.5\times10^{-6}$ Torr, $p_B=10^{-5}$ Torr, $\eta=0.005$, and $T=460$ K.

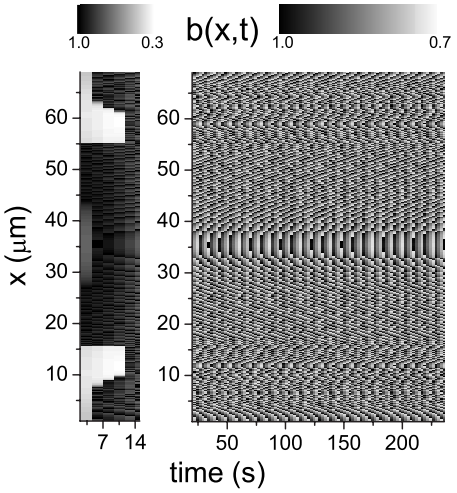

FIG. 10. Amplitude map of oxygen coverage b in the t,x plane in the regime of inhomogeneous oscillations. Here, $p_A=6.5\times10^{-6}$ Torr, $p_B=10^{-5}$ Torr, and $T=460$ K. The left-hand panel shows the development of the central nonuniform pattern and the expansion of irregular oscillations near the substrate boundaries at the initial stages of temporal evolution.

wave fronts observed in the amplitude maps of b in Fig. 10. These deformations are related to a transition to the regime of phase turbulence [30].

To deeper understand the origin of the standing waves, let us consider Eqs. (5) and (9) governing the spatiotemporal evolution of the system. In the development of the wave instability, the property of the CO coverage a to adjust the surface state plays a key role. This is demonstrated by the temporal evolution of a and n presented in Fig. 9. One can clearly see the development of inhomogeneous spatial profiles from the initial uniformly distributed $a(x)=a_p$. The decrease of a inside $\mathcal{C}$ is produced by the initial plateaulike distribution of n in this region. As a consequence, the parabolic concave shape of $a(x)$ leads to a negative second derivative $\partial^2 a/\partial x^2$ close to $x=x_\pm$. To see the effect of $\partial^2 a/\partial x^2<0$ on the wave properties, we consider a modified equation for b which can be derived in the vicinity of $\boldsymbol{\xi}_p$ on the basis of (5) and (9):

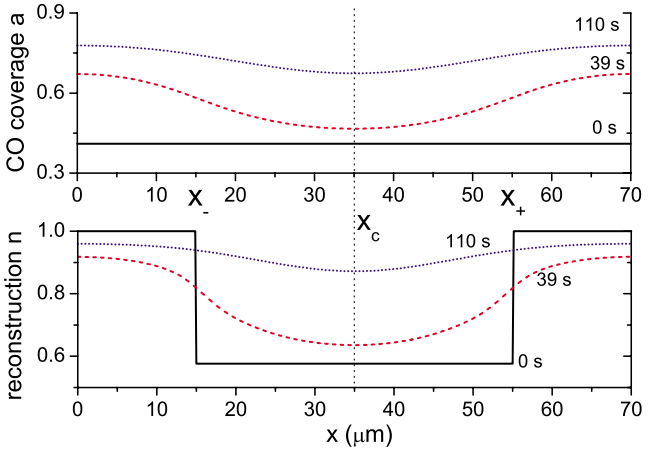

FIG. 9. (Color online) Time evolution of spatial profiles of the surface geometry described by n and of the CO coverage a. The initial n distribution is steplike with $n=n_p=0.57$ inside the central region $\mathcal{C}$ of a length $2\Delta=40$ μm with $x_c=35$ μm and $n=1$ beyond this region. The initial CO coverage $a(x)=a_p=0.41$ is homogeneous. Here $p_A=6.5\times10^{-6}$ Torr, $p_B=10^{-5}$ Torr, $\eta=0.005$, and $T=460$ K.

$$\frac{\partial^2 b}{\partial t^2} \approx \frac{\partial^2 a}{\partial x^2}(2n_p\tilde{p}_B - \tilde{r}A_s)b + f_0. \tag{12}$$

Here $f_0\approx -2n_p\tilde{p}_B(1-a)\partial^2 a/\partial x^2$. In the region $\mathcal{C}$, the expression for $\partial^2 a/\partial x^2$ can be approximated by a parabola

$$\partial^2 a/\partial x^2 \approx -\alpha_1(x-x_c)^2+\alpha_0, \tag{13}$$

with the curvature determined by the parameter α_1.

Furthermore, close to the hex/1×1 interfaces, we have $-\alpha_1(x_c-x)^2+\alpha_0=-\alpha(x)<0$. As a result, in the interface region the time-dependent part of the solution of (12) has the form of a standing wave,

$$b(x,t) = b_0\cos[\eta(x)t+\eta_0],$$

$$\eta(x) = \sqrt{\alpha(x)(2n_p\tilde{p}_B - \tilde{r}A_s)}. \tag{14}$$

The parameters η_0 and b_0 can be found from the boundary conditions $b(x_\pm,t)=b_>\cos(\omega t)$. Here $b_>(t)=b_>\cos(\omega t)$ is the oxygen coverage in the (1×1) areas beyond $\mathcal{C}$ which is assumed to be homogeneous for simplicity. The frequency ω is the oscillation frequency of the system. With these boundary conditions, close to the interface ($|x-x_c|\sim\Delta$), we have

$$b(x,t) = b_>\cos[\omega t+\delta\phi(x,t)], \tag{15}$$

where the function $\delta\phi(x,t)\sim\alpha_1[\Delta^2-(x-x_c)^2]t/\Delta$ describes the deformation of the homogeneous wave profile due to a

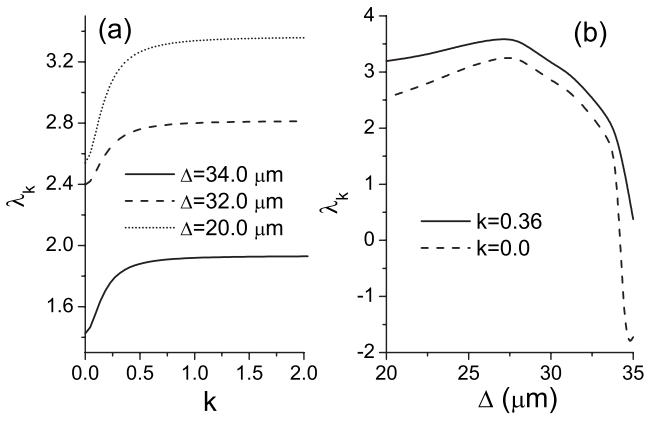

FIG. 11. (a) Dispersion of the real part of the Floquet exponent λ_k for different values of the half-width Δ of the reconstructed region $\mathcal{C}$. (b) λ_k as a function of Δ for different k. Here $p_A=6.4\times10^{-6}$ Torr, $p_B=10^{-5}$ Torr, and $T=460$ K.

nonzero curvature α_1 from (13). As the phase deformation $\delta\phi(x,t)$ is controlled by α_1, the oscillations of $\alpha_1(t)$ during the periodic cycles result in the inhomogeneous wave front oscillating with the constant frequency ω which is shown in the right-hand panel of Fig. 10.

In order to test the Benjamin-Feir instability characterized by an unstable oscillating state with respect to inhomogeneous perturbations, we have calculated the Floquet exponents for different wave numbers k. For the analysis of the spatially inhomogeneous states, we introduce the Fourier transforms $\xi_k=(a_k,n_k,b_k)^T$ and $f_i(k)$,

$$f_i(k)=\frac{1}{N_x}\sum_x f_i(a,n,b)\exp(-ikx)=f_i(a_k,n_k,b_k), \quad (16)$$

where the range of the wave numbers $k=2\pi l/L_x$ $(l=1,\ldots,N_x)$ is determined by the periodic boundary conditions $\boldsymbol{\xi}(x)=\boldsymbol{\xi}(x+L_x)$.

For a state represented by the vector $\boldsymbol{\xi}^0=(a_0,n_0,b_0)^T$ oscillating with a period T and described by (5) and (9), the analysis of the Floquet exponents can be reduced to the solution of the eigenvalue problem with the Jacobian $G_k=[g_{i,j}(k)]$ where $g_{i,j}(k)=\partial f_i(k)/\partial\xi_{kj}|_{\xi_k^0}$. The condition $\lambda_k<0$ implies the stability of $\boldsymbol{\xi}^0$ with respect to small inhomogeneous perturbations $\delta\boldsymbol{\xi}_k$. In contrast to this, the opposite condition $\lambda_k>0$ corresponds to the instability of the homogeneous oscillating state and to the appearance of modulation in the system.

Figure 11 presents the behavior of the maximal real part of the Floquet exponent $\lambda_k=\max\{\mathrm{Re}\,\lambda_k^1,\mathrm{Re}\,\lambda_k^2,\mathrm{Re}\,\lambda_k^3\}$ which occurs under a variation of the length Δ. One can clearly see that the decrease of Δ leads to a strong increase of λ_k for all values of k [Fig. 11(a)]. The positive λ_k for nonzero k indicates the formation of the inhomogeneous state presented in Figs. 8 and 10. Moreover, Fig. 11(b) shows that the bulklike oscillation state which develops in an initially homogeneous region $\mathcal{C}$ of a maximal length $\Delta=35$ μm, is unstable with respect to inhomogeneous perturbations. On such a substrate, the uniform oscillations cannot be destroyed by homogeneous perturbations which is reflected in $\lambda_k(k=0)<0$ in Fig. 11(b). In contrast, due to the positive $\lambda_k(k\neq0)$, the inhomogeneous perturbations diverge and lead to spatially modulated oscillations.

The principal feature of λ_k is its almost dispersionless (flat) character which can be clearly seen in Fig. 11(a). Specifically, for all values of Δ we obtain an initial increase of λ_k at small k, with a further saturation to the maximal constant value which occurs for larger $k>0.5$ [Fig. 11(a)]. This "flat-band"-character is in strong contrast to the dispersion λ_k usually obtained in the modeling of the global coupling for Pt(110) [10,11]. In the latter case, λ_k has a distinct well-defined maximum at a certain $k=k_0$ which corresponds to the appearance of spatial clusters with k_0 modulation. In our case, due to the flatness of λ_k at larger k, no distinctly leading mode can be formed. Instead, all possible k modulations can exist in such an unstable system. This is the key reason for a highly irregular form of the standing waves in Fig. 8. Although keeping the basic features related to the central symmetry, the irregular wave profiles are strongly sensitive to the initial state of the substrate and to the initial spatial distributions of the adsorbate coverage, and in this sense they are random. In the real systems, the type of irregular profile can be pinned by surface defects, such as steps and surface imperfections, with possible further random changes caused by the noise in the system.

In fact, the obtained spatiotemporal evolution of the irregular oscillations on the substrate is consistent with the development of irregular patterns on spatially separated patches typically observed on Pt(100). It should be noted that the inhomogeneous oscillating states and standing waves have been previously discussed for CO oxidation on Pt(110) where the main mechanism responsible for these phenomena is the coupling through the gas phase [10–12]. In contrast to Pt(110), on Pt(100) the inhomogeneities in the surface geometry play a central role. Such inhomogeneities lead to the nucleation of adsorbate islands and to a decisive role of the boundaries between geometrically different surface areas in the formation of standing waves and irregular oscillations.

VI. CONCLUSIONS

We have studied the CO adsorption and catalytic CO oxidation on inhomogeneous Pt(100) surfaces which contain structurally different hex and (1×1) domains. In our model, the structural surface transformation is described in terms of a bistability characterized by a coexistence of the reconstructed and 1×1 surface areas. The bistable region terminates in the critical cusp point which can be approached at higher temperatures and pressures. Due to significant increase of the fluctuations, the behavior in the vicinity of the cusp point should be qualitatively different from the hysteresis-type behavior typically observed in the experiments under ultrahigh vacuum conditions. We have studied the nucleation and growth of CO islands on inhomogeneous substrate, a process driven by the difference in the desorption properties of CO in the hex and 1×1 phases. We have also

performed the analysis of the oscillation behavior on the surface during the CO oxidation. The surface inhomogeneities lead to the Benjamin-Feir instability and to the irregular standing waves of adsorbate coverage. The obtained deformations of the wave fronts is a direct consequence of structural inhomogeneities typical for Pt(100) which allows us to gain deeper insight into the nature of irregular oscillations on this type of surfaces.

[1] J. M. White, Science **218**, 429 (1982).
[2] V. Fiorentini, M. Methfessel, and M. Scheffler, Phys. Rev. Lett. **71**, 1051 (1993).
[3] R. J. Behm, P. A. Thiel, P. R. Norton, and G. Ertl, J. Chem. Phys. **78**, 7437 (1983).
[4] P. A. Thiel, R. J. Behm, P. R. Norton, and G. Ertl, J. Chem. Phys. **78**, 7448 (1983).
[5] A. Hopkinson, J. M. Bradley, X.-C. Guo, and D. A. King, Phys. Rev. Lett. **71**, 1597 (1993).
[6] R. Imbihl and G. Ertl, Chem. Rev. **95**, 697 (1995).
[7] M. P. Cox, G. Ertl, and R. Imbihl, Phys. Rev. Lett. **54**, 1725 (1985).
[8] M. Eiswirth, P. Möller, K. Wetzl, R. Imbihl, and G. Ertl, J. Chem. Phys. **90**, 510 (1989).
[9] R. Imbihl, M. P. Cox, and G. Ertl, J. Chem. Phys. **84**, 3519 (1986).
[10] M. Falcke, H. Engel, and M. Neufeld, Phys. Rev. E **52**, 763 (1995).
[11] M. Bär, M. Hildebrand, M. Eiswirth, M. Falke, H. Engel, and M. Neufeld, Chaos **4**, 499 (1994).
[12] F. Mertens, R. Imbihl, and A. Mikhailov, J. Chem. Phys. **101**, 9903 (1994).
[13] G. Veser, F. Mertens, A. S. Mikhailov, and R. Imbihl, Phys. Rev. Lett. **71**, 935 (1993).
[14] N. Khrustova, G. Veser, A. Mikhailov, and R. Imbihl, Phys. Rev. Lett. **75**, 3564 (1995).
[15] P. Thostrup, E. Christoffersen, H. T. Lorensen, K. W. Jacobsen, F. Besenbacher, and J. K. Norskov, Phys. Rev. Lett. **87**, 126102 (2001).
[16] M. I. Monine, L. M. Pismen, and R. Imbihl, J. Chem. Phys. **121**, 11332 (2004).
[17] R. Imbihl, M. P. Cox, G. Ertl, H. Müller, and W. Brenig, J. Chem. Phys. **83**, 1578 (1985).
[18] V. N. Kuzovkov, O. Kortlüke, and W. von Niessen, J. Chem. Phys. **108**, 5571 (1998); O. Kortlüke, V. N. Kuzovkov, and W. von Niessen, *ibid.* **110**, 11523 (1999).
[19] V. P. Zhdanov and B. Kasemo, Surf. Sci. Lett. **513**, L385 (2002).
[20] N. Pavlenko, R. Imbihl, J. W. Evans, and Da-Jiang Liu, Phys. Rev. E **68**, 016212 (2003); N. Pavlenko, J. W. Evans, Da-Jiang Liu, and R. Imbihl, *ibid.* **65**, 016121 (2001).
[21] V. P. Zhdanov and B. Kasemo, Surf. Sci. Rep. **39**, 25 (2000).
[22] K. Krischer, M. Eiswirth, and G. Ertl, J. Chem. Phys. **96**, 9161 (1992).
[23] R. P. H. Gasser and E. B. Smith, Chem. Phys. Lett. **1**, 457 (1967).
[24] M. Bär, Ch. Zülicke, M. Eiswirth, and G. Ertl, J. Chem. Phys. **96**, 8595 (1992).
[25] V. N. Kuzovkov, O. Kortlüke, and W. von Niessen, Phys. Rev. E **66**, 011603 (2002).
[26] A. J. Bray, Adv. Phys. **43**, 357 (1994).
[27] M. Hildebrand, M. Ipsen, A. S. Mikhailov, and G. Ertl, New J. Phys. **5**, 61 (2003).
[28] R. Imbihl, Prog. Surf. Sci. **44**, 185 (1993).
[29] J. V. Barth, G. Constantini, and K. Kern, Nature (London) **437**, 671 (2005).
[30] Y. Kuramoto, Prog. Theor. Phys. **63**, 1885 (1980).